

Research Paper

Thermodynamic Analysis of Radiating Nanofluids Mixed Convection within Concentric Pipes Filled with a Porous Medium

Oluwole Daniel MAKINDE¹*, Fazle MABOOD²),
Waqar Ahmed KHAN³), Anuoluwa Esther MAKINDE⁴)

¹) *Faculty of Military Science, Stellenbosch University*
Private Bag X2, Saldanha 7395, South Africa

²) *Department of Information Technology, Fanshawe College London*
ON, Canada; e-mail: mabood1971@yahoo.com

³) *Department of Mechanical Engineering, College of Engineering,*
Prince Mohammad Bin Fahd University
Al Khobar 31952, Kingdom of Saudi Arabia; e-mail: wkhan_2000@yahoo.com

⁴) *Faculty of Engineering, Stellenbosch University*
Private Bag X1, Matieland 7602, South Africa; e-mail: anu.makinde7@gmail.com

*Corresponding Author e-mail: makinded@gmail.com

In this study, the entropy generation resulting from heat and mass transfer of water-based nanofluid through an annulus within two concentric vertical pipes filled with a porous medium is investigated. This study considers the effects of thermal radiation, viscous dissipation, thermal buoyancy, and axial pressure gradient in addition to heat and mass transfer. Brownian motion and thermophoresis have been introduced through the Buongiorno model. The similarity solution was used to solve nonlinear ordinary differential equations. The Runge-Kutta-Fehlberg method is used to solve these equations with the related boundary conditions. The effects of pertinent parameters such as pressure gradient, thermal radiation, viscosity parameter, thermophoretic parameter, Brownian motion parameter, and Eckert number are investigated numerically. This study found that the Bejan number increases as the viscosity parameter increases and decreases as the other active parameters increase. As the radiation parameter, thermophoretic parameter, Brownian parameter, and Eckert number increase, the Nusselt number decreases. The total entropy generation rate is found to increase with the fluid viscosity rate, Grashof number, thermal Biot number, and variable pressure gradient. However, the Bejan number is found to decrease with these parameters, as well as the Prandtl number.

Keywords: nanofluid; concentric pipes; mixed convection; thermal radiation; porous medium; entropy analysis.

1. INTRODUCTION

In recent years, convective flow in a concentric annulus has attracted much attention owing to its importance for engineering applications such as thermal energy storage systems, cooling of electronic components, oil and gas drilling wells, and extruders. In all these applications, the concentric cylinders can be stationary, in motion, or one stationary and the other in motion during operation. WATANABE *et al.* [1] studied the fluid flow within concentric cylinders with vertical axes, both theoretically and experimentally. They discovered that the movement of the inner cylinder alters the flow structure. Additionally, they found that the critical Reynolds number at the free surface fluctuates with a rapid increase in both the velocity components and the kinetic energy. MAKINDE [2] numerically studied the steady axial Couette flow of Ostwald-de Waele power-law fluids between concentric cylinders. The outer cylinder, which is fixed, exchanges heat with the surrounding environment according to Newton's law of cooling, while the inner cylinder, which is isothermal, moves in an axial direction. The work revealed the thermal criticality for the onset of instability in the flow environment. It was reported that the entire circulating structure and thermal decomposition strongly depend on the embedded thermophysical parameters. The heat transfer capability of a viscoelastic fluid in an annular flow within two rotating concentric cylinders was analytically examined by LORENZINI *et al.* [3] using the Giesekus model. It was found that a rise in the Brinkmann number may lead to the asymptotic behavior of the Nusselt number. COELHO and PINTO [4] theoretically examined the impact of an embedded porous medium in conduit flows of a non-Newtonian fluid and obtained a generalized Brinkmann number that is valid for any flow regime to calculate the proportion of frictional heat and heat exchange at the wall.

The thermodynamic enactment of industrial systems can be heightened with different aspects linked to entropy generation. Thermodynamic irreversibility and entropy generation are connected, and this happens in practically all flow and heat exchange activities. BEJAN [5] investigated the impact of entropy generation minimization on fluid flow and heat transfer in a thermal device. MAKINDE and EEGUNJOBI [6, 7] theoretically examined the inherent irreversibility in both forced and mixed convective flow between two concentric pipes in the presence of a magnetic field, porous medium and thermal radiation. Other researchers [8–19] have investigated entropy generation in fluid flow with heat and mass transfer under different physical situations.

Recently, heat transfer in nanofluid became an extensive research area amongst scientists and authors because nanofluid can substantially boost the heat transfer features in the base fluid. It is a known fact that the heat transfer process plays an incredibly significant role in engineering and industries. Hence,

these fluids have applications in industrial processes, nuclear reactors, solar collectors, solar thermal systems, photovoltaic systems, coolants, biomedicine, and electronic devices. Primarily, CHOI and EASTMAN [20] introduced nanofluid phenomena, in which they concluded that thermal conductivity rises tremendously in the presence of nanoparticles in the base liquid. KHAN and POP [21] theoretically studied the impact of nanoparticles on the flow structure of nanofluid past a linearly stretching sheet surface. The problem of non-Newtonian nanofluids convection over a radially stretching rotating disk was investigated by SHAHZAD *et al.* [22]. FERDOWS *et al.* [23] numerically examined the combined effects of heat source and suction on the thermal boundary layer of a nanofluid past a moving permeable surface. MABOOD *et al.* [24] explored Arrhenius pre-exponential factor law for electro-magnetohydrodynamics (EMHD) of non-Newtonian nanofluids over the thin needle with Robinson's condition. Other authors [25–29] have studied the heat mass transfer enhancement capability of nanofluids under different physical situations.

CHAKRABORTY and RAY [30] combined the first and second laws of thermodynamics to optimize the thermal-hydraulic performance of laminar fully developed flow through square ducts with rounded corners. The study showed that the optimal duct geometry strongly depends on the thermal-hydraulic constraints as well as the objective functions. They found that the rounded corner ducts produce better performance under constant heat input and uniform temperature along the periphery of the duct at a given axial location. Additionally, they observed that the perfectly square ducts offer the best performance in terms of the first law objective function. LORENZINI and SUZZI [31] studied the fully developed steady laminar flow of a Newtonian liquid through a microchannel subject to different thermal boundary conditions. They used the entropy generation number and the constrained total heat transfer area to evaluate the effect of smoothing the corners of an initially rectangular cross-section on the thermal-hydraulic performance. They found that smoothing the corners of the microchannel led to an improvement in its performance.

From a literature survey, it was found that the irreversibility analysis for mixed radiative convection flows in porous regimes within concentric pipes has not been thoroughly investigated yet, which is, in fact, the extension of [6]. Hence, the present work aims to fill this gap in the literature. Nanofluid in two concentric pipes consisting of porous media has many important applications, namely, in heat exchange systems in metallurgical and petrochemical procedures, underground discarding of nuclear wastes, and thermal converters with a porous liner. MAKINDE [2] also evaluated the effect of various parameters on the velocity profile, temperature profile, concentration profile, skin friction, Nusselt and Sherwood numbers, entropy generation rate, and the Bejan number. The results of these evaluations are presented with graphs and discussed in the study.

2. MODEL PROBLEM

We consider the steady flow of an incompressible variable viscosity nanofluid through the annulus inside two concentric vertical pipes filled with a porous medium in addition to the united action of thermal buoyancy and axial pressure gradient. The inner pipe surface was assumed to be smooth and at a constant high temperature (T_0) due to a heat-generating mechanical process within the pipe, while the outer surface of the pipe was able to exchange heat with the surrounding environment through convection, in accordance with Newton’s law of cooling, as shown in Fig. 1. To describe the flow of the fluid through a porous medium with high velocity, the Brinkmann-Darcy-Forchheimer model was employed. The Forchheimer model incorporates two terms that indicate the viscous effect and the inertial effect. The model utilizes the square root of permeability as the corresponding length characteristics are in agreement with the linearized Darcy law at low velocities, while the non-dimensional coefficient in the quadratic term is used to represent the inertial effect.

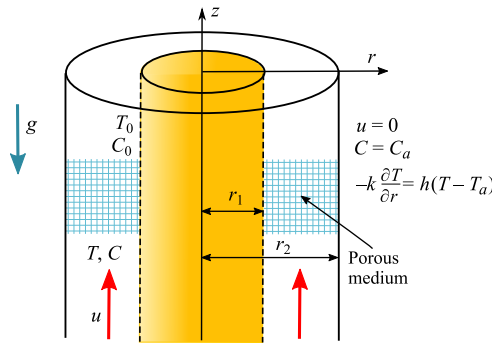


FIG. 1. Schematic diagram of the model problem.

With these assumptions, the continuity, momentum, energy, and volumetric entropy generation rate equations take the following form [6]:

$$(2.1) \quad \frac{\partial u}{\partial z} = 0,$$

$$(2.2) \quad -\frac{\partial P}{\partial z} + \frac{1}{r} \frac{\partial}{\partial r} \left(r \mu(T) \frac{\partial u}{\partial r} \right) + g\beta (T - T_a) - \frac{\mu(T)u}{K} - \frac{\rho c u^2}{\sqrt{K}} = 0,$$

$$(2.3) \quad \frac{k}{r} \frac{\partial}{\partial r} \left(r \frac{\partial T}{\partial r} \right) - \frac{\partial q_r}{\partial r} + \mu(T) \left(\frac{\partial u}{\partial r} \right)^2 + \frac{\mu(T)u^2}{K} + \frac{c u^3}{\sqrt{K}} + \tau \left(D_B \frac{\partial C}{\partial r} \frac{\partial T}{\partial r} + \frac{D_T}{(T_0 - T_a)} \left(\frac{\partial T}{\partial r} \right)^2 \right) = 0,$$

$$(2.4) \quad \frac{D_B}{r} \frac{\partial}{\partial r} \left(r \frac{\partial C}{\partial r} \right) + \frac{D_T}{(T_0 - T_a)r} \frac{\partial}{\partial r} \left(r \frac{\partial T}{\partial r} \right) - b(C - C_a) = 0,$$

$$(2.5) \quad E_G = \frac{k}{(T_0 - T_a)^2} \left(1 + \frac{16\sigma^* T_a^3}{3kk^*} \right) \left(\frac{\partial T}{\partial r} \right)^2 + \frac{\mu(T)}{(T_0 - T_a)} \left(\frac{\partial u}{\partial r} \right)^2 \\ + \frac{\mu(T)u^2}{(T_0 - T_a)K} + \frac{cu^3}{(T_0 - T_a)\sqrt{K}} + \frac{RD_B}{(T_0 - T_a)} \frac{\partial C}{\partial r} \frac{\partial T}{\partial r} + \frac{RD_B}{(C_0 - C_a)} \left(\frac{\partial C}{\partial r} \right)^2,$$

where b is the reaction rate, τ is the specific heat ratio, D_B is the nanoparticles' mass diffusivity, D_T is the thermophoresis coefficient, R is the nanoparticles' mass transfer irreversibility coefficient, z is the axial length, K is the porous medium's permeability, c is the Forchheimer inertial coefficient, r is the radial coordinate, T denotes the temperature of the fluid, u stands for axial velocity component while other velocity components are zero, ρ is the density of the nanofluid, k is the thermal conductivity of the nanofluid, P is the fluid pressure, C is the nanoparticles concentration, C_0 is the nanoparticles concentration at the inner cylinder surface while C_a is the nanoparticles concentration at the outer cylinder surface, β represents the volumetric thermal enlargement coefficient, E_G is the volumetric entropy production (generation) rate, and g represents acceleration as a result of gravity.

The dynamical temperature-dependent viscosity $\mu(T)$ is taken as

$$(2.6) \quad \mu(T) = \mu_0 e^{-m(T-T_a)},$$

where μ_0 is the dynamic viscosity of the nanofluid at ambient temperature T_a such that $T_a < T_0$, and m is the viscosity variation coefficient. In line with the Roseland approximation [18, 19], the local radiative heat flux term for an optically thick gray nanofluid is given by

$$(2.7) \quad q_r = -\frac{4\sigma^*}{3k^*} \frac{\partial T^4}{\partial r} \approx -\frac{16\sigma^* T_a^3}{3k^*} \frac{\partial T}{\partial r},$$

where $T^4 \approx 4T_a^3 T - 3T_a^4$ (using Taylor series estimation), and k^* is the mean absorption coefficient and σ^* is the Stefan-Boltzmann constant. The relevant boundary conditions at both the inner slip surface and the outer convective cooling surface are as follows:

$$(2.8) \quad u = \frac{\mu(T_0)}{\delta} \frac{\partial u}{\partial r}, \quad T = T_0, \quad C = C_0, \quad \text{at } r = r_1,$$

$$(2.9) \quad u = 0, \quad -k \frac{\partial T}{\partial r} = h(T - T_a), \quad C = C_a, \quad \text{at } r = r_2,$$

where h is the heat transfer coefficient, δ is the slip coefficient, and r_1, r_2 are the inside and outside radii, respectively. The following non-dimensional variables and parameters are introduced into the model Eqs. (2.1)–(2.9):

$$\begin{aligned}
 \bar{P} &= \frac{\rho r_1^2 L P}{\mu_0^2}, & w &= \frac{\rho u r_1}{\mu_0}, \\
 \eta &= \frac{r - r_1}{r_1 L}, & Z &= \frac{z}{r_1 L}, \\
 \theta &= \frac{T - T_a}{T_0 - T_a}, & L &= \frac{r_2 - r_1}{r_1}, \\
 \varepsilon &= -\frac{\partial \bar{P}}{\partial Z}, & \gamma &= m(T_0 - T_a), \\
 \text{Gr} &= \frac{\rho g \beta r_1^3 L^2 (T_0 - T_a)}{\mu_0^2}, & \text{Ns} &= \frac{E_g r_1^2 L^2}{k}, \\
 \text{Pr} &= \frac{\mu_0 c_p}{k}, & \text{Bi} &= \frac{h r_1 L}{k}, \\
 \text{Ec} &= \frac{\mu_0^2}{\rho^2 r_1^2 c_p (T_0 - T_a)}, & \text{Nr} &= \frac{16 \sigma^* T_a^3}{3 k k^*}, \\
 \phi &= \frac{C - C_a}{C_0 - C_a}, & \chi &= \frac{L^2 r_1^2 b}{D_B}, \\
 \text{Da} &= \frac{K}{r_1^2 L^2}, & F &= \frac{c L^2 r_1^2}{\sqrt{K}}, \\
 \text{Nb} &= \frac{\tau D_B (C_0 - C_a)}{k}, & \text{Nt} &= \frac{\tau D_T}{k}, \\
 \lambda &= \frac{\mu_0}{\delta r_1 L}, & H_1 &= \frac{R}{\tau}.
 \end{aligned}
 \tag{2.10}$$

The dimensionless controlling equations, together with the suitable boundary conditions, can be written as

$$\frac{d^2 w}{d\eta^2} - \gamma \frac{dw}{d\eta} \frac{d\theta}{d\eta} + \left(\frac{L}{L\eta + 1} \right) \frac{dw}{d\eta} + (\text{Gr} \theta - F w^2 + \varepsilon) e^{\gamma \theta} - \frac{w}{\text{Da}} = 0,
 \tag{2.11}$$

$$\begin{aligned}
 (1 + \text{Nr}) \frac{d^2 \theta}{d\eta^2} + \left(\frac{L}{L\eta + 1} \right) \frac{d\theta}{d\eta} + \text{Pr Ec} e^{-\gamma \theta} \left(\frac{dw}{d\eta} \right)^2 \\
 + \frac{\text{Pr Ec}}{\text{Da}} e^{-\gamma \theta} w^2 + F \text{Pr Ec} w^3 + \text{Nb} \frac{d\phi}{d\eta} \frac{d\theta}{d\eta} + \text{Nt} \left(\frac{d\theta}{d\eta} \right)^2 = 0,
 \end{aligned}
 \tag{2.12}$$

$$(2.13) \quad \frac{d^2\phi}{d\eta^2} + \left(\frac{L}{L\eta + 1}\right) \frac{d\phi}{d\eta} + \frac{Nt}{Nb} \left[\frac{d^2\theta}{d\eta^2} + \left(\frac{L}{L\eta + 1}\right) \frac{d\theta}{d\eta} \right] - \chi\phi = 0,$$

$$(2.14) \quad Ns = (1 + Nr) \left[\frac{d\theta}{d\eta} \right]^2 + Pr Ec e^{-\gamma\theta} \left(\frac{dw}{d\eta} \right)^2 + \frac{Pr Ec e^{-\gamma\theta} w^2}{Da} \\ + F Pr Ec w^3 + H_1 Nb \left(\frac{d\phi}{d\eta} \frac{d\theta}{d\eta} + \left(\frac{d\phi}{d\eta} \right)^2 \right),$$

with

$$(2.15) \quad w(0) = \lambda e^{-\gamma} \frac{dw}{d\eta}(0), \quad \theta(0) = 1, \quad \phi(0) = 1,$$

$$(2.16) \quad w(1) = 0, \quad \frac{d\theta}{d\eta}(1) = -Bi \theta(1), \quad \phi(1) = 0,$$

where γ is the decrease rate of fluid viscosity due to temperature variation, Nr is the thermal radiation parameter, Da is the Darcy number, F is the Forchheimer inertial parameter, λ is the slip parameter, ε is the pressure gradient variable, Gr is the Grashof number, C_p represents the specific heat at a steady pressure, L denotes the concentric cylinder annulus parameter, Pr is the Prandtl number, Ec refers to the Eckert number, Bi represents the thermal Biot number, Nb is the Brownian motion parameter, Nt is the thermophoresis parameter, χ is the reaction rate parameter, H_1 corresponds to irreversibility parameters due to nanoparticles diffusion while η denotes the non-dimensional annulus within the two cylinders. Other relevant parameters of engineering interest are skin friction (Cf), Nusselt number (Nu), Sherwood number (Sh) and can be expressed as

$$(2.17) \quad Cf = \frac{\rho r_1^2 L \tau_w}{\mu_0^2} = e^{-\gamma\theta(\eta)} \left. \frac{dw(\eta)}{d\eta} \right|_{\eta=0,1}, \\ Nu = \frac{r_1 L q_w}{k(T_0 - T_a)} = - (1 + Nr) \left. \frac{d\theta(\eta)}{d\eta} \right|_{\eta=0,1}, \\ Sh = \frac{r_1 L q_m}{D_B(C_0 - C_a)} = - \left. \frac{d\phi(\eta)}{d\eta} \right|_{\eta=0,1},$$

where

$$\tau = \mu(T) \left. \frac{du}{dr} \right|_{r_1, r_2}, \quad q_w = -k \left(1 + \frac{16 \sigma^* T_a^3}{3kk^*} \right) \left. \frac{dT}{dr} \right|_{r=r_1 r_2}, \\ q_m = -D_B \left. \frac{dC}{dr} \right|_{r=r_1, r_2}.$$

The Bejan number (Be) is defined as the ratio of heat and mass transfer irreversibility to the total entropy generation rate given as

$$(2.18) \quad \text{Be} = \frac{N_1 + N_3}{N_s} = \frac{N_1 + N_3}{N_1 + N_2 + N_3} = \frac{1}{1 + Q},$$

where $Q = \frac{N_2}{N_1 + N_3}$ is the irreversibility ratio, $N_1 = (1 + Nr) \left[\frac{d\theta}{d\eta} \right]^2$ represents the heat transfer irreversibility, and the irreversibility due to combined effects of viscous dissipation and porous medium resistance heating is given as

$$N_2 = \text{Pr Ec} e^{-\gamma\theta} \left(\frac{dw}{d\eta} \right)^2 + \frac{\text{Pr Ec} e^{-\gamma\theta} w^2}{\text{Da}} + F \text{Pr Ec} w^3$$

while the irreversibility due to nanoparticles diffusion rate is given as

$$N_3 = H_1 Nb \left(\frac{d\phi}{d\eta} \frac{d\theta}{d\eta} + \left(\frac{d\phi}{d\eta} \right)^2 \right).$$

3. NUMERICAL PROCEDURE

The dimensionless governing Eqs. (2.11)–(2.14) coupled with the boundary conditions (2.15)–(2.16) are treated numerically via the Runge-Kutta-Fehlberg (RKF) with the shooting technique that considers several values of parameters. Then, an investigation exploring the dynamic parameters' influences on

Table 1. Comparison of $w(\eta)$ values between exact solution [1] and RKF-45 when $L = 2$, $\text{Da} = \infty$, $\text{Gr} = F = \gamma = \lambda = Nb = Nt = 0$.

η	MAKINDE and EEGUNJOBI [6] (exact solution)	Present results (RKF-45)
0.0	0.000000	0.000000
0.1	0.055478	0.055478
0.2	0.093135	0.093136
0.3	0.116407	0.116406
0.4	0.127513	0.127513
0.5	0.127964	0.127961
0.6	0.118842	0.118840
0.7	0.100942	0.100942
0.8	0.074871	0.074870
0.9	0.041099	0.041099
1.0	0.000000	0.000000

the non-dimensional velocities, temperature, concentration, skin frictions, Nusselt, Sherwood, and Bejan numbers can be carried out. The innermost step size of $\Delta\eta = 0.01$, having accurateness up to the 5th decimal place, is reserved as the convergence criterion. To validate the precision of the developed model, the numeric outcomes of $w(\eta)$ are estimated for various inputs of η , as presented in Table 1, and found in the best agreement with [6].

4. RESULTS AND DISCUSSION

In this study, the heat and mass transfer of water-based nanofluid flow through concentric cylindrical annulus associated with slip and convective boundary conditions is performed numerically. Table 1 compares the axial velocity results from MAKINDE and EEGUNJOBI [6] to validate the numerical model. It demonstrates that the study’s numerical results are very similar to those of earlier published articles. The effects of pertinent parameters on non-dimensional axial velocity are presented in Figs. 2 and 3. It can be seen in Fig. 2a that with an increase in the concentric gap parameter, the fluid velocity in the annular gap decreases. This may be attributed to the existence of wall shear stress, which has a great impact on the flow motion. It can be seen in Fig. 2b that the main driving force is the pressure gradient. The non-dimensional velocity within the annulus gap rises as the pressure gradient rises. The slip parameter also helps in enhancing the axial velocity within the annulus gap. The buoyancy effect on the flow is analyzed through the Grashof number in Fig. 2b. As seen in Fig. 2b, an increase in the Grashof number leads to an increase in the temperature difference, which leads to an increase in the non-dimensional velocity. Increasing the temperature difference also helps with flow convection. The Forchheimer inertial

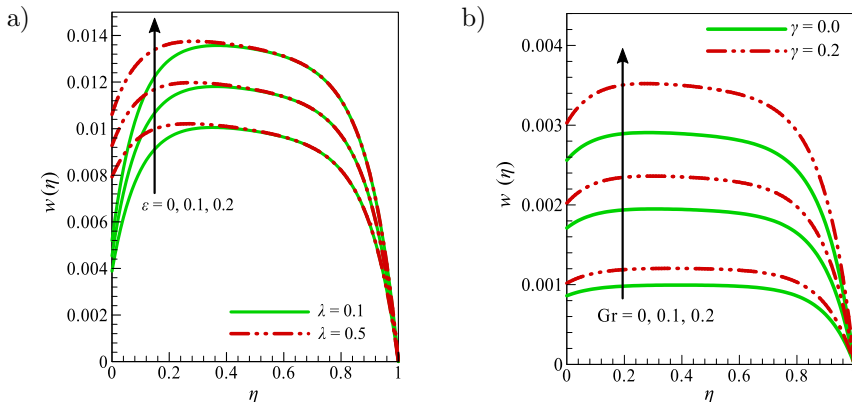


FIG. 2. Velocity distribution in the axial direction for different values of (a) pressure gradient and slip parameters and (b) rate of fluid viscosity and Grashof number.

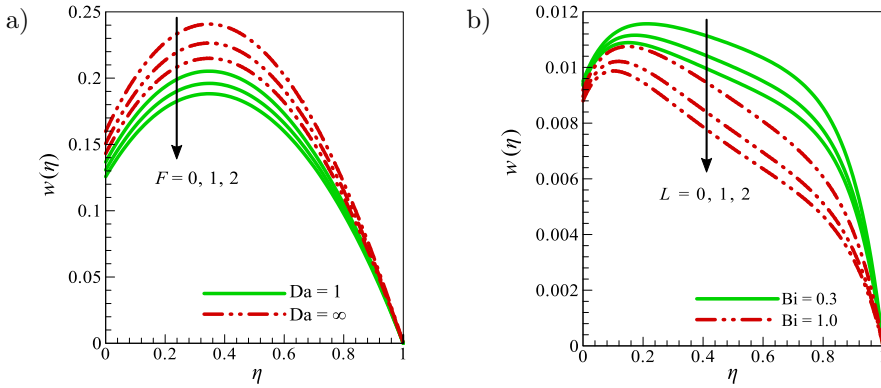


FIG. 3. Velocity distribution in the axial direction for different values of (a) Forchheimer inertial and Darcy numbers and (b) concentric cylinder annulus and thermal Biot parameters.

parameter connects the pressure loss caused by friction in a porous medium to the velocity of the flow inside the medium.

The influence of the Forchheimer inertial parameter on the velocity distribution is depicted in Fig. 3a. With a rise in the Forchheimer inertial parameter, a decreasing effect is observed near the gap's center. Figure 3a also shows the effect of the Darcy number on the velocity distribution. The permeability of a porous medium increases with an increase in the Darcy number. As a result, the flow through the porous medium encounters less resistance. As a result, the velocity rises. Figure 3b depicts the influence of the concentric gap parameter on the non-dimensional velocity. In the absence of the Forchheimer inertial parameter, the axial velocity is higher at the inner surface and decreases with an increasing Forchheimer inertial parameter. It increases between inner and outer surfaces, reaches up to the maximum, and then decreases to zero. The Darcy parameter dictates the flow of a fluid through the porous medium. For small values of the Darcy parameter, the axial velocity is lower and increases for higher values of the Darcy number. Figure 3b also displays the impact of the Biot number on the axial velocity. For smaller values of the Biot number, the axial velocity is found to be higher and decreases with increasing Biot number.

Figure 4a presents the effects of the pressure gradient parameter and Darcy number on the non-dimensional temperature. It can be seen that an increase in the pressure gradient causes the fluid molecules to increase and thereby raise the temperature contour. In addition, increase in the Darcy number increases the non-dimensional temperature at the outer surface. However, the non-dimensional temperature decreases between the inner and outer surfaces. Figure 4b presents the effects of concentric gap parameters and reaction rate parameters on the non-dimensional concentration of nanoparticles. As the concentric gap parameter is increased, the non-dimensional temperature declines,

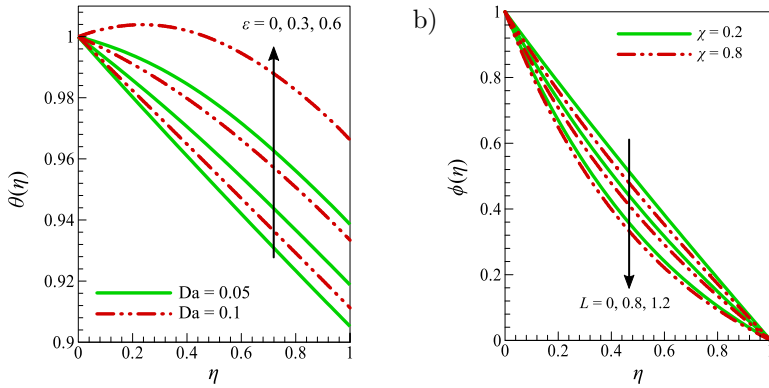


FIG. 4. Temperature distribution in the axial direction for different values of (a) pressure gradient parameter and Darcy number and (b) concentric cylinder annulus and reaction rate parameters.

which is most noticeable towards the pipe’s outside. The reaction rate parameter also helps in reducing the non-dimensional temperature between the surfaces.

Figure 5 describes the variation in skin friction with slip parameters for different values of pressure gradient, concentric gap parameter, and Darcy number on the inner and outer surfaces. Skin friction portrays the frictional force at the inner and outer boundaries between a fluid and a wall. At both boundaries, the skin friction reduces with the slip parameter. At the inner boundary, the skin friction increases with Darcy’s number. It is because a rise in Darcy’s number causes a support in velocity gradients at the surface, which increases the skin friction coefficient. The pressure gradient parameter tends to increase the skin friction at the inner surface, see Fig. 5a. Negative skin friction can be no-

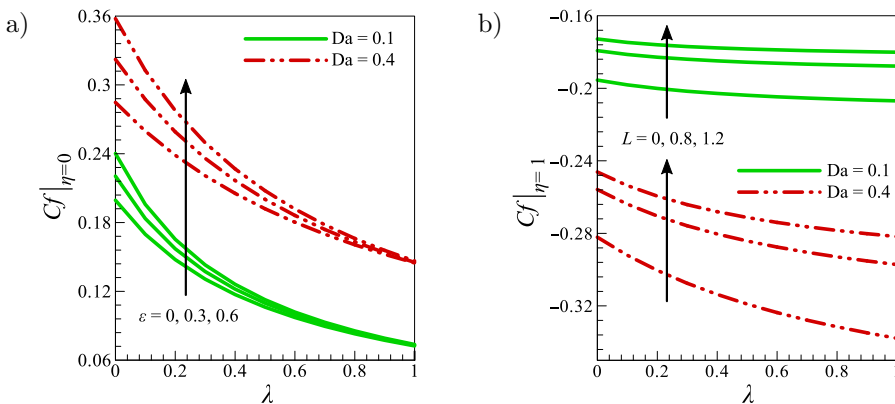


FIG. 5. Variation in skin friction with slip parameter for different values of (a) pressure gradient parameter and Darcy number on the inner surface and (b) concentric cylinder annulus parameter and Darcy number on the outer surface.

ticed when skin friction is examined at the outer surface, see Fig. 5b. When the friction force increases with decreasing load, negative friction coefficients appear. The concentric gap parameter increases the skin friction at the outer surface.

At the inner surface, the Nusselt number increases with thermal radiation and thermal Biot number. However, the Nusselt number decreases with increasing viscous dissipation, Fig. 6a. At the outer surface, the Nusselt number increases with an increase in each parameter, as shown in Fig. 6b. The total heat input into the fluid through the surface is the sum of radiation and convection heat transfer. This total heat transfer rate is converted into a non-dimensional number, known as the Nusselt number. The Biot number describes the obstacle to heat transfer “within” a solid body. The Biot number is defined as the ratio of a surface’s external resistance to convection energy exchange to its internal resistance to transmitting energy by conduction. A low Biot number signifies low conduction resistance and, thus, very low-temperature gradients within the body, leading to the lumped system analysis, which assumes a uniform temperature distribution throughout the body. This effect of thermal radiation and Biot number is explained graphically in Fig. 6.

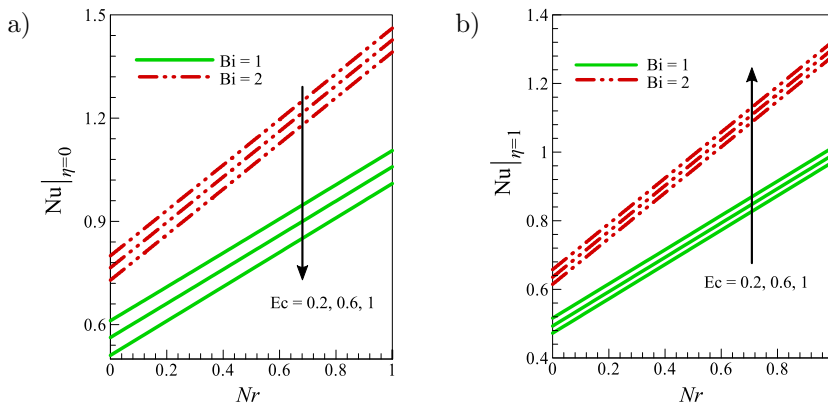


FIG. 6. Variation in Nusselt number with thermal radiation parameter for different values of Eckert and thermal Biot numbers on (a) the inner surface and (b) the outer surface.

The Sherwood number measures the mass convection at the surface. It is defined as the ratio of mass diffusivity to convective mass transfer. So, the Sherwood number decreases at the lower surface as the Brownian motion parameter Nb grows (Fig. 7a), but at the outer surface, the Sherwood number increases with an increase in Nb (Fig. 7b) for convective cooling. Nanofluid is a two-phase flow in which nanoparticles move about randomly, increasing energy exchange rates. The nanoparticles improve the heat transfer surface area. Brownian motion corresponds to the random movement of nanoparticles in the base fluid. This

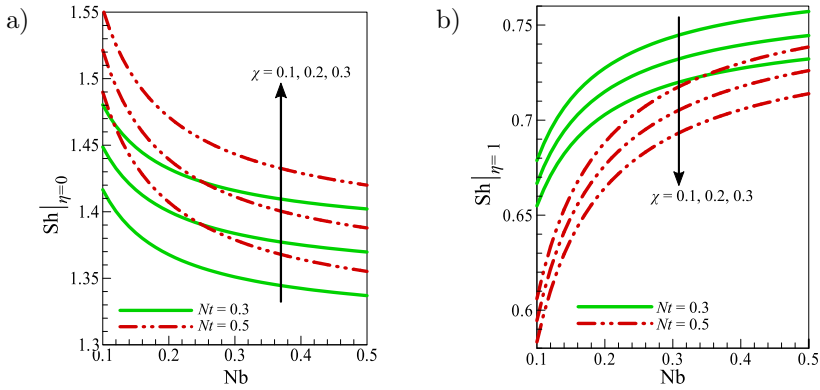


FIG. 7. Variation in Sherwood number with Brownian motion parameter for different values of thermophoresis and reaction rate parameters on (a) the inner surface and (b) the outer surface.

random movement accelerates the nanoparticles' collision with base fluid molecules. Consequently, molecules' kinetic energy is converted into thermal energy and hence temperature rises. As Nb increases, the temperature rises, but concentration falls within the boundary layer, as demonstrated in Fig. 7. Due to an increase in the reaction rate parameter, the mass transfer rate increases at the inner surface while decreasing at the outer surface.

Figure 8a presents the effects of fluid viscosity rate, pressure gradient, and Grashof number on the non-dimensional entropy generation rate profile. The porous medium leads to a high disorder of the flow particles inside the annulus and increases the entropy generation, while little or no effect of the restrictive medium is detected at the outer surface. The fluid viscosity also tends to enhance the entropy generation rate, as shown in Fig. 8a. The entropy generation rate due to fluid friction increases as the pressure gradient rises. Because of the viscous

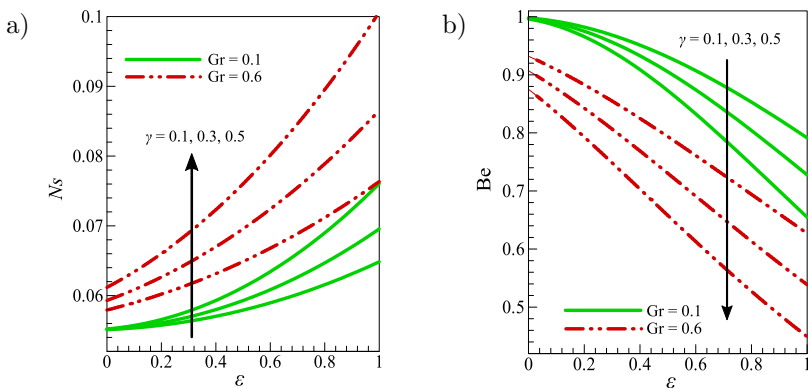


FIG. 8. Effects of fluid viscosity rate and Grashof number in the presence of variable pressure gradient on (a) the total entropy generation rate and (b) the Bejan number.

friction between the walls and the fluid, entropy generation due to fluid friction is expected to be higher on the wall than anywhere else in the channel. The fluid motion accelerates, and convective heat transfer rises as the Grashof number increases. As a result, the entropy generation rate increases with the Grashof number. The Bejan number reveals the proportion of overall entropy generation that is produced by thermal irreversibility. Consequently, it defines the entropy generated by heat transfer and fluid friction. When the Bejan number for any thermal system is close to one, it means that thermal entropy generation takes precedence over frictional entropy generation. However, $Be = 0$ corresponds to the case in which the irreversibility is dominated by the fluid friction effects. Also, $Be = 0.5$ corresponds to the case in which the heat transfer irreversibility and the fluid friction irreversibility are equal. Figure 8b shows that, in each case, the Bejan number is greater than 0.5. Therefore, the irreversibility due to heat transfer dominates over friction. At the outer surface, every parameter tends to reduce the Bejan number.

The effect of the concentric gap parameter on the entropy generation rate is seen in Fig. 9a. As the concentric gap parameter is increased, the entropy generation rate increases at the inner wall and near the channel center. Meanwhile, from the middle of the gap to the outer pipe, there is no effect. The restricting medium gradually fades away from the inner pipe toward the outside pipe, according to this finding. An increase in the irreversibility parameters due to nanoparticle concentration also tends to raise the total entropy generation rate, whereas the slip parameter shows little effect on the entropy generation rate, see Fig. 9a. The effects of the same parameters on the Bejan number are presented in Fig. 9b. It reveals that heat transfer makes a major contribution to the entropy generation rate. Like the total entropy generation rate, the Bejan number

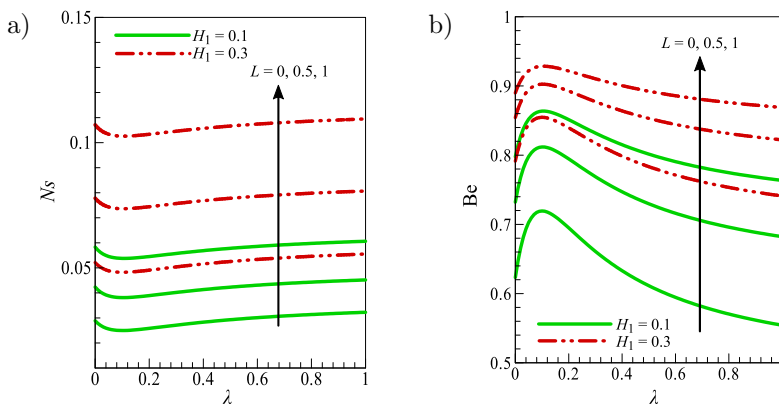


FIG. 9. Effects of concentric cylinder annulus and irreversibility parameters due to nanoparticles concentration in the presence of slip on (a) the total entropy generation rate and (b) the Bejan number.

also increases with an increase in the concentric gap as well as heat transfer irreversibility parameters.

Figure 10a shows how the entropy generation number varies with thermal radiation depending on the Darcy number and Forchheimer inertial parameter. It is observed that the entropy generation rate escalates with an increase in the radiation and Darcy parameters, whereas an upsurge in Forchheimer inertial parameter lowers the entropy generation rate. As the value of thermal radiation rises, more heat flux is absorbed into the fluid, resulting in increased entropy generation due to heat transfer, and therefore the entropy generation rate due to heat transfer dominates. A rise in Darcy’s number improves the permeability of the medium, which increases the entropy generation rate. Figure 10b illustrates the variation in Bejan number with thermal radiation parameter and Darcy number. The thermal radiation parameter enhances heat transfer irreversibility and thus raises the Bejan number. The Darcy number (Da) shows the relative effect of the medium’s permeability vs. its cross-sectional area in fluid dynamics across porous media. Consequently, it reduces irreversibility due to heat transfer, and as a result, the Bejan number decreases with increasing Darcy number. The irreversibility parameter due to Forchheimer inertial parameter also tends to increase the Bejan number.

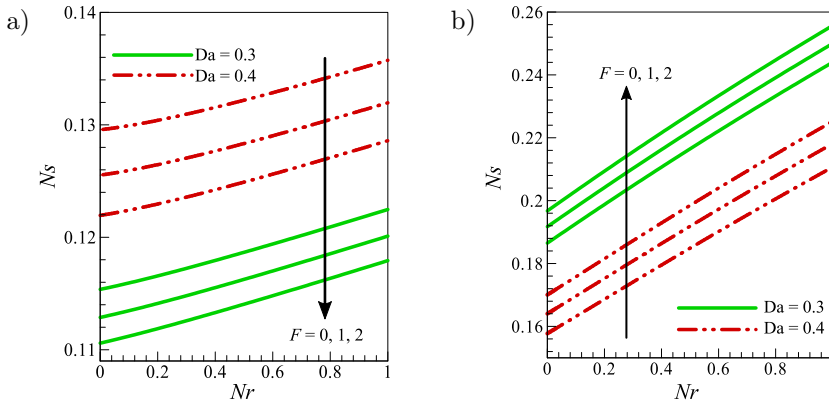


FIG. 10. Effects of Darcy number and Forchheimer inertial parameter in the presence of thermal radiation on (a) the total entropy generation rate and (b) the Bejan number.

Brownian motion and thermophoresis are heat and mass transfer mechanisms that cause nanoparticles to migrate in the direction of falling temperature and concentration gradients. The effects of these nanofluid parameters on the non-dimensional entropy generation rate and Bejan number are displayed in Fig. 11a and 11b, respectively. This is performed in the presence of viscous dissipation. Since incremental thermal diffusion and temperature rise are caused by the Brownian motion of nanoparticles, the total entropy generation rate de-

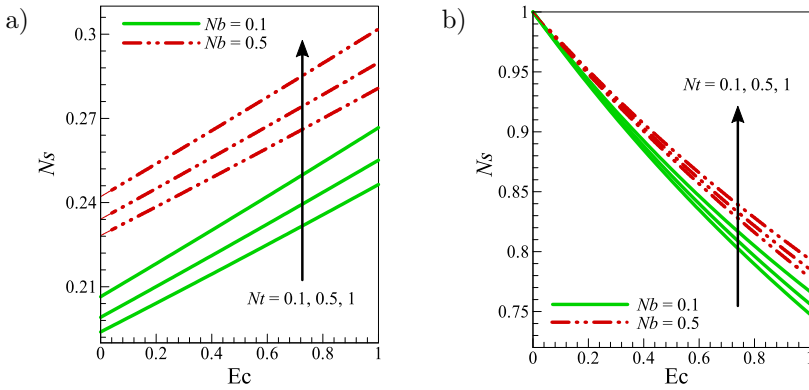


FIG. 11. Effects of thermophoresis and Brownian motion parameters in the presence of viscous dissipation on (a) the total entropy generation rate and (b) the Bejan number.

increases with increasing Brownian motion parameters, and hence Bejan number decreases. Similarly, when nanoparticles travel from a hotter to a cooler zone, the thermophoretic effect occurs, distributing heat in the thermal boundary layer. Consequently, an increase in the thermophoresis parameter tends to increase the total entropy generation rate, and hence Bejan number rises. The viscous dissipation helps in increasing irreversibility due to friction which increases the total entropy generation rate and decreases the Bejan number, Eq. (2.18).

The Biot number represents the ratio of the resistance to heat transfer from the inner surface to the outer surface. A reaction rate is a useful diagnostic tool. We can develop strategies to optimize production by learning how fast items are made and what causes responses to slow down. Figure 12a shows the impact of reaction rate on the total entropy generation for two values of Prandtl numbers while the Biot number is increasing. It can be observed that the entropy

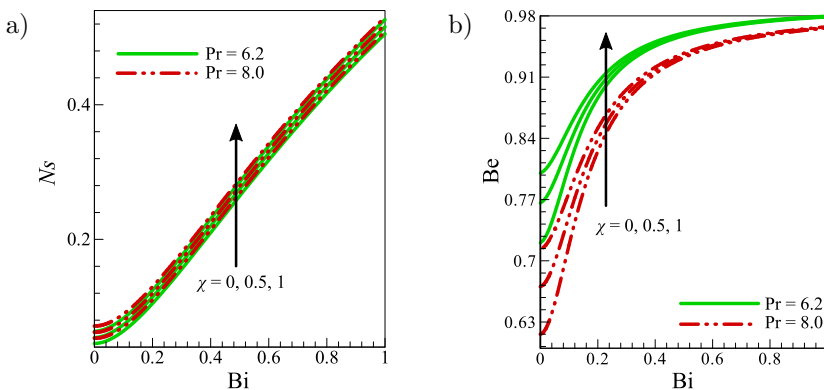


FIG. 12. Effects of Prandtl number and reaction rate parameter on (a) the total entropy generation rate and (b) the Bejan number.

generation rate increases with an increasing Biot number. It is due to an increase in resistance to heat transfer. However, reaction rate and Prandtl number show negligible effects on the total entropy generation rate. Figure 12b displays the variation in the Bejan number with both the Biot number and reaction rate. Both parameters tend to increase in Bejan number due to an increase in the heat transfer irreversibility. However, an increase in the Prandtl number reduces the Bejan number.

5. CONCLUSION

This study combines the principles of thermodynamics, fluid dynamics, and heat transfer to understand the behavior of nanofluids. It focuses on the thermal-hydraulic performance of the system, including the heat transfer, fluid flow, and thermodynamic behavior of the nanofluids within the concentric pipes. The presence of an embedded porous medium enhances the nanofluid temperature profiles and lessens the thermal resistance of the system. The following is a summary of our findings:

- The axial velocity increases with Grashof and Darcy numbers, fluid viscosity, pressure gradient and slip parameters, while Forchheimer inertial, concentric cylinder annulus and thermal Biot parameters tend to decrease the axial velocity.
- The non-dimensional temperature increases with the pressure gradient parameter and Darcy number.
- The non-dimensional concentration of nanofluid decreases with concentric cylinder annulus and reaction rate parameters.
- The skin friction increases with Darcy number, pressure gradient and concentric cylinder annulus parameters but decreases with slip parameter.
- The thermal radiation parameter and Biot number boost the Nusselt number, while viscous dissipation reduces the Nusselt number at the inner surface and improves the Nusselt number at the outer surface.
- The Brownian motion parameter reduces the mass transfer rate at the inner surface while it improves the mass transfer rate at the outer surface.
- The thermophoresis and reaction rate parameters help in improving the mass transfer rates while they decrease the mass transfer rates at the outer surface.
- An increase in the radiation and Darcy parameters boost the entropy generation rate, whereas Forchheimer inertial parameter lowers the rate.

It is important to note that the appropriate selection of the thermo-physical and nanofluid parameters would minimize entropy generation in engineering

thermal and fluid flow applications such as concentric pipe heat exchangers with mixed convection in a porous medium for best performance. The results of the study can be used to optimize the thermal-hydraulic performance of the system and to design more efficient heat exchangers, solar collectors, and other thermal systems that use nanofluids and porous media.

REFERENCES

1. WATANABE T., TOYA Y., NAKAMURA I., Development of free surface flow between concentric cylinders with vertical axes, *Journal of Physics: Conference Series*, **14**: 9–19, 2005, doi: 10.1088/1742-6596/14/1/002.
2. MAKINDE O.D., Thermal analysis of a reactive generalized Couette flow of power law fluid between concentric cylindrical pipes, *The European Physical Journal Plus*, **129**(2): 270 (9 pages), 2014, doi: 10.1140/epjp/i2014-14270-4.
3. LORENZINI M., DAPRÀ I., SCARPRI G., Heat transfer for a Giesekus fluid in a rotating concentric annulus, *Applied Thermal Engineering*, **122**: 118–125, 2017, doi: 10.1016/j.applthermaleng.2017.05.013.
4. COELHO P.M., PINHO F.T., A generalized Brinkman number for non-Newtonian duct flows, *Journal of Non-Newtonian Fluid Mechanics*, **156**(3): 202–206, 2009, doi: 10.1016/j.jnnfm.2008.07.001.
5. BEJAN A., Second-law analysis in heat transfer and thermal design, *Advance in Heat Transfer*, **15**: 1–58, 1982, doi: 10.1016/S0065-2717(08)70172-2.
6. MAKINDE O.D., EEGUNJOBI A.S., Inherent irreversibility of mixed convection within concentric pipes in a porous medium with thermal radiation, *Journal of Mathematical and Fundamental Sciences*, **53**(3): 395–414, 2021, doi: 10.5614/j.math.fund.sci.2021.53.3.5.
7. MAKINDE O.D., EEGUNJOBI A.S., Entropy analysis of a variable viscosity MHD Couette flow between two concentric pipes with convective cooling, *Engineering Transactions*, **68**(4): 317–334, 2020, doi: 10.24423/engtrans.1104.20200720.
8. MONALEDI R.L., MAKINDE O.D., Entropy generation analysis in a microchannel Poiseuille flows of nanofluid with nanoparticles injection and variable properties, *Journal of Thermal Analysis and Calorimetry*, **143**: 1855–1865, 2021, doi: 10.1007/s10973-020-09919-x.
9. NAYAK M.K., MABOOD F., DOGONCHI A.S., RAMADAN K.M., TLILI I., KHAN W.A., Entropy optimized assisting and opposing nonlinear radiative flow of hybrid nanofluid, *Waves in Random and Complex Media*, 22 pages, 2022, doi: 10.1080/17455030.2022.2032474.
10. MABOOD F., FAROOQ W., ABBASI A., Entropy generation analysis in the electro-osmosis-modulated peristaltic flow of Eyring-Powell fluid, *Journal of Thermal Analysis and Calorimetry*, **147**(5): 3815–3830, 2022, doi: 10.1007/s10973-021-10736-z.
11. SHAW S., MABOOD F., MUHAMMAD T., NAYAK M.K., ALGHAMDI M., Numerical simulation for entropy optimized nonlinear radiative flow of GO-Al₂O₃ magneto nanomaterials with auto catalysis chemical reaction, *Numerical Methods for Partial Differential Equations*, **38**(3): 329–358, 2022, doi: 10.1002/num.22623.
12. MABOOD F., FATUNMBI E.O., BENOS L., SARRIS I.E., Entropy generation in the magneto-hydrodynamic Jeffrey nanofluid flow over a stretching sheet with wide range of engineering

- application parameters, *International Journal of Applied and Computational Mathematics*, **8**(3): 98, 2022, doi: 10.1007/s40819-022-01301-9.
13. NAYAK M.K., MABOOD F., KHAN W.A., MAKINDE O.D., Cattaneo-Christov double diffusion on micropolar magneto cross nanofluids with entropy generation, *Indian Journal Physics*, **96**(1): 193–208, 2022, doi: 10.1007/s12648-020-01973-3.
 14. SHAW S., CHAMKHA A.J., WAKIF A., MAKINDE O.D., NAYAK M.K., Effects of Wu's slip and non-uniform source/sink on entropy optimized radiative magnetohydrodynamic up/down flow of nanofluids, *Journal of Nanofluids*, **11**(3): 305–317, 2022, doi: 10.1166/jon.2022.1840.
 15. SATHYANARAYANAN S.U.D, MABOOD F., JAMSHED W., MISHRA S.R., NISAR K., PATNAIK P.K., PRAKASH M., ABDEL-ATY A.H., ZAKARYA M., Irreversibility process characteristics of variant viscosity and conductivity on hybrid nanofluid flow through Poiseuille microchannel: A special case study, *Case Studies in Thermal Engineering*, **27**: 101337, 2021, doi: 10.1016/j.csite.2021.101337.
 16. NAYAK M.K., MABOOD F., TLILI I., DOGONCHI A.S., KHAN W.A., Entropy optimization analysis on nonlinear thermal radiative electromagnetic Darcy-Forchheimer flow of SWCNT/MWCNT nanomaterials, *Applied Nanoscience*, **11**(2): 399–418, 2021, doi: 10.1007/s13204-020-01611-8.
 17. AZAM A., MABOOD F., XU T., WALY M., TLILI I., Entropy optimized radiative heat transportation in axisymmetric flow of Williamson nanofluid with activation energy, *Results in Physics*, **19**: 103576, 2020, doi: 10.1016/j.rinp.2020.103576.
 18. BERREHAL H., SOWMYA G., MAKINDE O.D., Shape effect of nanoparticles on MHD nanofluid flow over a stretching sheet in the presence of heat source/sink with entropy generation, *International Journal of Numerical Methods for Heat & Fluid Flow*, **32**(5): 1643–1663, 2022, doi: 10.1108/HFF-03-2021-0225.
 19. NAYAK M.K., SHAW S., KHAN M.I., MAKINDE O.D., CHU Y.M., KHAN S.U., Interfacial layer and shape effects of modified Hamilton's Crosser model in entropy optimized Darcy-Forchheimer flow, *Alexandria Engineering Journal*, **60**(4): 4067–4083, 2021, doi: 10.1016/j.aej.2021.02.010.
 20. CHOI S.U.S., EASTMAN J.A., Enhancing thermal conductivity of fluids with nanoparticles, [in:] *Developments and Applications of Non-Newtonian Flows, FED-V.231/MD, ASME, D.A. Siginer, H.P. Wang [Eds.]*, **66**: 99–105, 1995.
 21. KHAN W.A., POP I., Boundary-layer flow of a nanofluid past a stretching sheet, *International Journal of Heat and Mass Transfer*, **53**(11–12): 2477–2483, 2010, doi: 10.1016/j.ijheatmasstransfer.2010.01.032.
 22. SHEHZAD S.A., MABOOD F., RAUF A., IZADI M., ABBASI F.M., Rheological features of non-Newtonian nanofluids flows induced by stretchable rotating disk, *Physica Scripta*, **96**(3): 035210, 2021, doi: 10.1088/1402-4896/abd652.
 23. FERDOWS M., SHAMSHUDDIN M.D., SALAWU S.O., ZAIMI K., Numerical simulation for the steady nanofluid boundary layer flow over a moving plate with suction and heat generation, *SN Applied Sciences*, **3**(2): 1–11, 2021, doi: 10.1007/s42452-021-04224-0.
 24. MABOOD F., MUHAMMAD T., NAYAK M.K., WAQAS H., MAKINDE O.D., EMHD flow of non-Newtonian nanofluids over thin needle with Robinson's condition and Arrhenius pre-exponential factor law, *Physica Scripta*, **95**(11): 115219, 2020, doi: 10.1088/1402-4896/abc0c3.

25. KHAN W.A., MAKINDE O.D., KHAN Z.H., Non-aligned MHD stagnation point flow of variable viscosity nanofluids past a stretching sheet with radiative heat, *International Journal of Heat and Mass Transfer*, **96**: 525–534, 2016, doi: 10.1016/j.ijheatmasstransfer.2016.01.052.
26. ALI A.O., KHAMIS S.A., SEIF F.S., MAKINDE O.D., Entropy analysis of the unsteady Darcian nanofluid flow in a cylindrical pipe with a porous wall, *International Journal of Ambient Energy*, **43**(1): 7321–7329, 2022, doi: 10.1080/01430750.2022.2063382.
27. EEGUNJOBI A.S., MAKINDE O.D., Entropy analysis in an unsteady MHD flow of a radiating fluid through a vertical channel filled with a porous medium, *International Journal of Ambient Energy*, **43**(1): 6404–6416, 2022, doi: 10.1080/01430750.2021.2019112.
28. RIKITU B.H., MAKINDE O.D., ENYADENE L.G., Modeling heat transfer enhancement of Ferrofluid ($\text{Fe}_3\text{O}_4\text{-H}_2\text{O}$) flow in a microchannel filled with a porous medium, *Journal of Nanofluids*, **10**(1): 31–44, 2021, doi: 10.1166/jon.2021.1764.
29. ABBASI A., MABOOD F., FAROOQ W., HUSSAIN Z., Non-orthogonal stagnation point flow of Maxwell nano-material over a stretching cylinder, *International Communications in Heat and Mass Transfer*, **120**: 105043, 2021, doi: 10.1016/j.icheatmasstransfer.2020.105043.
30. CHAKRABORTY S., RAY S., Performance optimisation of laminar fully developed flow through square ducts with rounded corners, *International Journal of Thermal Sciences*, **50**(12): 2522–2535, 2011, doi: 10.1016/j.ijthermalsci.2011.06.006.
31. LORENZINI M., SUZZI N., The influence of geometry on the thermal performance of microchannels in laminar flow with viscous dissipation, *Heat Transfer Engineering*, **37**(13/14): 1096–1104, 2016, doi: 10.1080/01457632.2015.1111100.

Received June 21, 2022; accepted version April 20, 2023.



Copyright © 2023 The Author(s).

This is an open-access article distributed under the terms of the Creative Commons Attribution-ShareAlike 4.0 International ([CC BY-SA 4.0 https://creativecommons.org/licenses/by-sa/4.0/](https://creativecommons.org/licenses/by-sa/4.0/)) which permits use, distribution, and reproduction in any medium, provided that the article is properly cited. In any case of remix, adapt, or build upon the material, the modified material must be licensed under identical terms.